

H. Föll
print 1975

Formation and Nature of Swirl Defects in Silicon

H. Föll

Max-Planck-Institut für Metallforschung, Institut für Physik
D-7000 Stuttgart 80, Fed. Rep. Germany

B. O. Kolbesen

Siemens AG, Grundlagenentwicklung Halbleiter
D-8000 München 46, P.O.Box 460705, Fed. Rep. Germany

Received 4 June 1975/Accepted 19 August 1975

Abstract. Point defect agglomerates in dislocation-free silicon crystals, usually called “swirls”, have been investigated by means of high-voltage electron microscopy. It was found that a single swirl defect consists of a dislocation loop or a cluster of dislocation loops. By contrast experiments it could be shown that these loops are formed by agglomeration of self-interstitial atoms. Generally the loops have $a/2\langle 110 \rangle$ Burgers vectors, but in specimens with high concentrations of carbon ($\sim 10^{17} \text{ cm}^{-3}$) and oxygen ($\sim 10^{16} \text{ cm}^{-3}$) also dislocation loops including a stacking fault were observed. In crystals grown at growth rates higher than $v = 4 \text{ mm/min}$ no swirls are observed; lower growth rates do not markedly affect the size and shape of the dislocation loops. With decreasing impurity content (particularly of oxygen and carbon) the swirl density decreases, whereas the dislocation loop clusters become larger and more complex. A model is presented which describes the formation of swirls in terms of agglomeration of silicon self-interstitials and impurity atoms.

Index Headings: Self-interstitials in silicon – Swirls – Electron microscopy

In dislocation-free crystals of silicon specific defects, commonly called “swirls” or “swirl defects”, are frequently observed. They appear, e.g., after a Sirtl etch treatment [1] as shallow etch-pits in a spiral or cloudy arrangement. These defects may be detrimental to the operation of silicon semiconductor devices (see e.g. [2, 3]). Swirls are generally thought to arise from the agglomeration of point defects which were in thermal equilibrium at high temperatures. Their study is therefore not only of technological importance but may provide basic information on point defects in silicon.

The methods used to study the nature of swirls include: X-ray topography [4], especially after decoration with Cu or Li [2, 5], investigations of the etch patterns revealed after a preferential etch treatment with optical and scanning electron microscopes [6, 10], spreading-resistance measurements [7], and transmission electron microscopy (TEM) [8–11].

With the exception of TEM these methods yield only macroscopic informations about swirls, e.g., on the dependence of density and spatial distribution on growth conditions. The most extensive studies concerning those topics were performed by de Kock and coworkers [2, 5]. In [2] two types of swirls, which are often present simultaneously, could be distinguished, so-called “A-clusters” and “B-clusters”. Whereas “A-clusters” are large, “B-clusters” are small but present in a higher density and in a spatial distribution different from that of “A-clusters”. The notion “cluster” – although in general used for every kind of point defect agglomerates – should express de Kock’s feeling that both types of swirls are loose agglomerates of vacancies. We prefer in the following a more neutral denomination and distinguish between “A-swirls” and “B-swirls”.

Until recently microscopic informations about swirls were only given by the TEM investigations of Ravi

and Varker [8]. These authors found in swirl-rich regions of a crystal ordered precipitates of SiO₂ which they believed to be identical with the swirls.

New insights into the macroscopic nature of swirls were obtained by combining high-voltage transmission electron microscopy (HVEM) with a large-area technique of specimen thinning [9, 10]. These investigations gave the result that A-swirls consist of complicated arrangements of dislocation loops. As reported in a recent note [11], these loops are of interstitial type, contrary to the prevailing view that swirls are vacancy clusters. From the interstitial nature of swirl defects it was concluded that self-interstitials are the predominant defects under equilibrium conditions near the melting point, a prediction made from the self-diffusion theory of Seeger and coworkers [12–14].

The present paper, which is based on our previous investigations [9–11], emphasizes the analysis of typical dislocation loops, applying the method described in [15]. The influence of the impurity content and of the crystal growth rate on the dislocation loops located below a swirl etch-hillock is investigated in more detail, and a model for nucleation and growth of swirls is presented.

1. Experimental Details

1.1. Specifications of the Silicon Crystals

The dislocation-free silicon crystals were grown by the floating-zone technique in argon or vacuum (~33 mm diameter; {111}-orientation; growth rate usually 3 mm/min; *n*- or *p*-type resistivity $\geq 50 \Omega\text{cm}$). The impurity contents of the crystals, as determined by IR-spectroscopy (oxygen and carbon) or neutron activation analysis¹ (other impurities, especially heavy metals) can be taken from Table 1.

¹ For the neutron activation analysis the authors are grateful to E. Haas and Miss H. Furtner of Siemens AG RT 21 (now KWU), Erlangen.

Table 1. Impurity contents of the crystals [atoms per cm³]

Crystal	Ambient	Oxygen	Carbon	Au	Cu	Other elements
AZ 1	Argon	10 ¹⁵	10 ¹⁶	5 · 10 ⁸	5 · 10 ¹¹	<10 ¹³
AZ 2	Argon	5 · 10 ¹⁵	5 · 10 ¹⁶	—	—	—
AZ 3 ^a	Argon	6 · 10 ¹⁵	1.2 · 10 ¹⁷	—	—	—
VZ 1	Vacuum	<5 · 10 ^{13b}	<2 · 10 ¹⁵	<10 ⁸	<3 · 10 ¹¹	<10 ¹³

^a This crystal was grown at successively increasing growth rates.

^b This detection limit was obtained by H. Neubrand, AEG-Telefunken, Frankfurt, Fed. Rep. Germany with a special ESR-oxygen determination method [16].

1.2. Specimen Preparation and High-Voltage Electron Microscopy

Specimens suitable for HVEM were obtained by the large-area thinning procedure as described by Kolbesen *et al.* [17]. This method yields discs with diameters between 30 mm and 50 mm and a uniform thickness of ~2 μm. With photochemical procedures it is possible to select a suitable area for a specimen (diameter = 1.8 mm in our case) [17]. Compared to specimens prepared in the usual way, e.g. by jet thinning techniques [18], this method offers two advantages, namely:

i) A very large area (the whole specimen) is transparent to the electron beam. This is necessary because the swirl density is very low (10⁵ cm⁻³ to 10⁷ cm⁻³; i.e. about one swirl in an area of 100 × 100 μm in a 2 μm thick foil) and therefore a large area has to be examined in order to find any swirl at all.

ii) A uniform thickness in the required range (2–3 μm in our case) may be achieved. In thinner foils too many dislocation loops would be lost by etching.

Observations were then carried out in a Hitachi HU 650 electron microscope at a beam voltage of 650 kV. The radiation damage by the high-energy electrons is very low and has little effect on the observations [19, 20].

2. Results

2.1. General Observations and Classifications of the Swirl Loops

On a specimen prepared from a swirl-rich region of the crystal, typically about 20–50 swirl etch-hillocks could be detected in the HVEM. In most cases dislocation loops, or complicated arrangements of dislocation loops (in the following named "swirl loops") were found below the hillocks (Figs 1–4). The density and size of the swirl loops were found to be strongly influenced by the impurity content of the crystals.

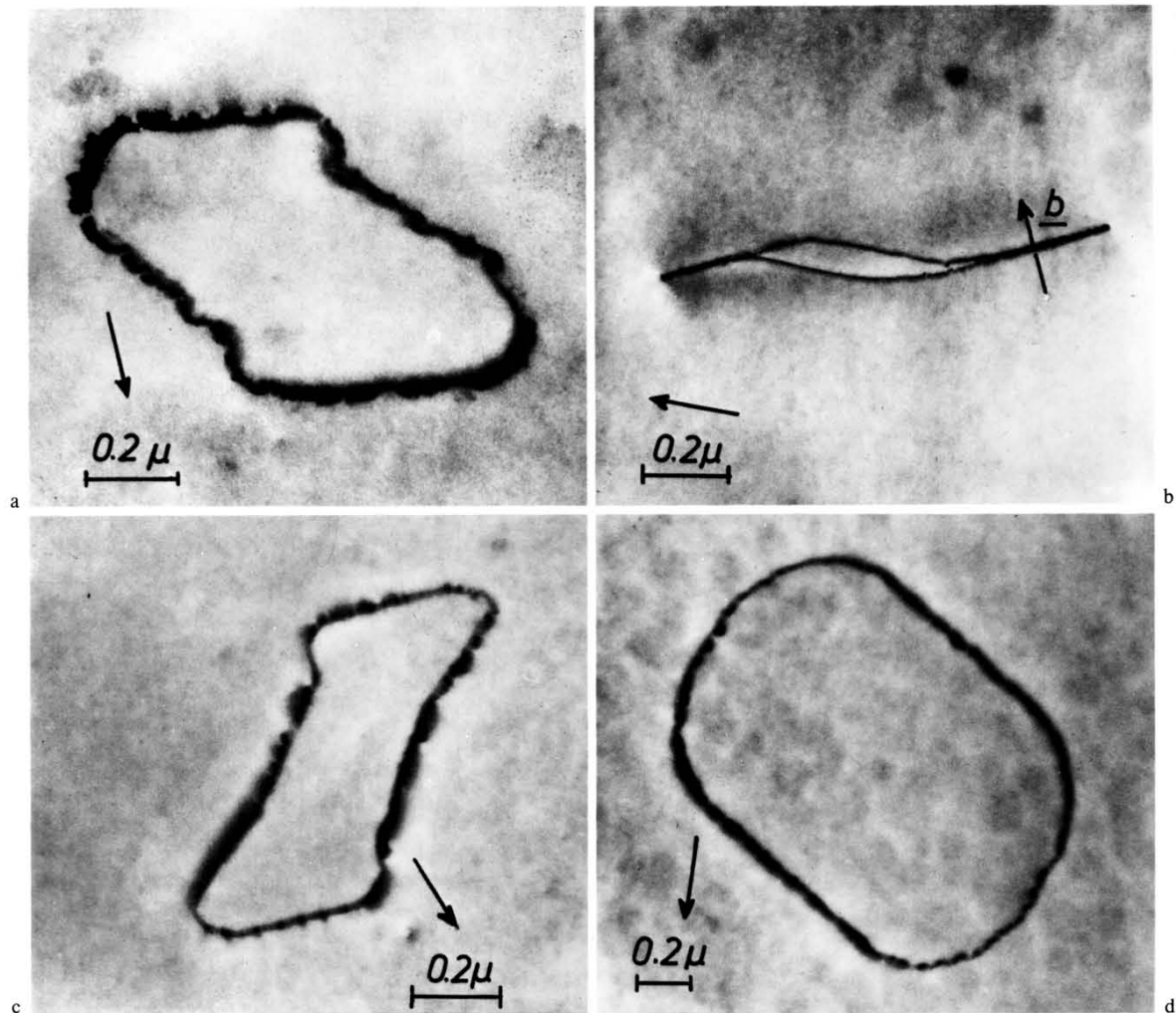


Fig. 1a–d. Typical examples of “single loops” observed in crystal AZ 2 and AZ 3. In (b) the projection of b onto the image plane is shown. Foil normal n is near $\{111\}$, and diffraction vector g is of $\{220\}$ type in this and in the following figures unless otherwise noted

As an example, the swirl density in crystal AZ 3 ($\sim 10^7 \text{ cm}^{-3}$) was about 10 times higher than in crystal VZ 1 ($\sim 10^6 \text{ cm}^{-3}$), whereas the size of the related dislocation loops was about 10 times smaller. The swirl loops in vacuum-grown material are generally more complicated than those in argon-grown crystals. We may roughly classify them into four categories.

i) “Single loops”. Some examples of single loops are shown in Fig. 1. Single loops are only found in the

crystals AZ 2 and AZ 3. Their mean diameters are about $0.5 \mu\text{m}$.

ii) “Loop clusters” of two or more loops which may have undergone reactions with each other, but each loop is well distinguishable from the others. Figure 2 shows some examples. The individual loops of a loop cluster in general have different Burgers vectors, indicating that they were created independently.

Loop clusters were found in the crystals AZ 1–AZ 3 in a rather limited number.

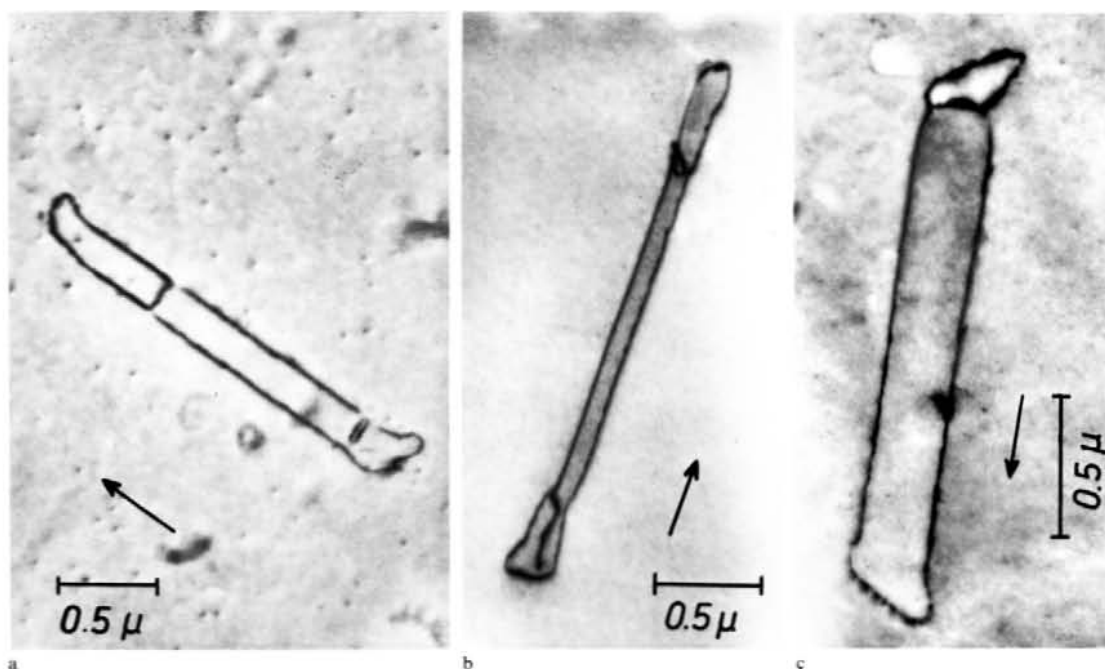


Fig. 2a-c. Typical examples of "loop clusters" observed in crystals AZ 1-AZ 3. Foil normal is near $\{110\}$ in (c)

iii) "Complicated arrangements", as shown in Fig. 3. The individual loops can in general no longer be distinguished from each other. In vacuum-grown material (crystal VZ 1) up to now only this type has been observed. In crystal AZ 1 complicated arrangements are predominant; only few loop clusters and no single loops were found. In the crystals AZ 2 and AZ 3 single loops and loop clusters predominate, complicated arrangements are found in a small number.

iv) "Faulted loops". In the specimen with the highest oxygen and carbon content (AZ 3) faulted loops were observed (Fig. 4). These loops can occur as single loops or as loops in a loop cluster. In the other crystals, apart from one case out of 70, no faulted loops were observed.

2.2. Common Features of Swirl Loops

The following features are common to nearly all swirl loops:

i) Most single loops are elongated parallel to a $\langle 110 \rangle$ -direction.

ii) Long and narrow dislocation dipoles (see, e.g., Fig. 3) are always of pure edge character.

iii) The tips of elongated single loops, as well as of loops in loop clusters, are often bowed away from the main direction in such a manner that they are of pure edge character (see, e.g., Fig. 1b, where a loop is seen edge-on).

iv) Swirl loops always exhibit an anomalous contrast, which indicates that they are decorated (not necessarily with impurities). In the case of vacuum-grown material (crystal VZ 1) this decoration could frequently be resolved into small dislocation loops. In the case of argon-grown crystals the decoration could not be resolved. (Since the samples used were relatively thick, the resolution power was not very high and small loops with diameters below 200 \AA would at best appear as a blurred black dot.) The dislocation then appears in a hemlike contrast or attended by black dots, depending on the diffraction conditions (Fig. 5). It is very likely that the decoration in this case also consists of small dislocation loops. In no case the decoration of the swirl loops could be attributed to precipitates of impurities.

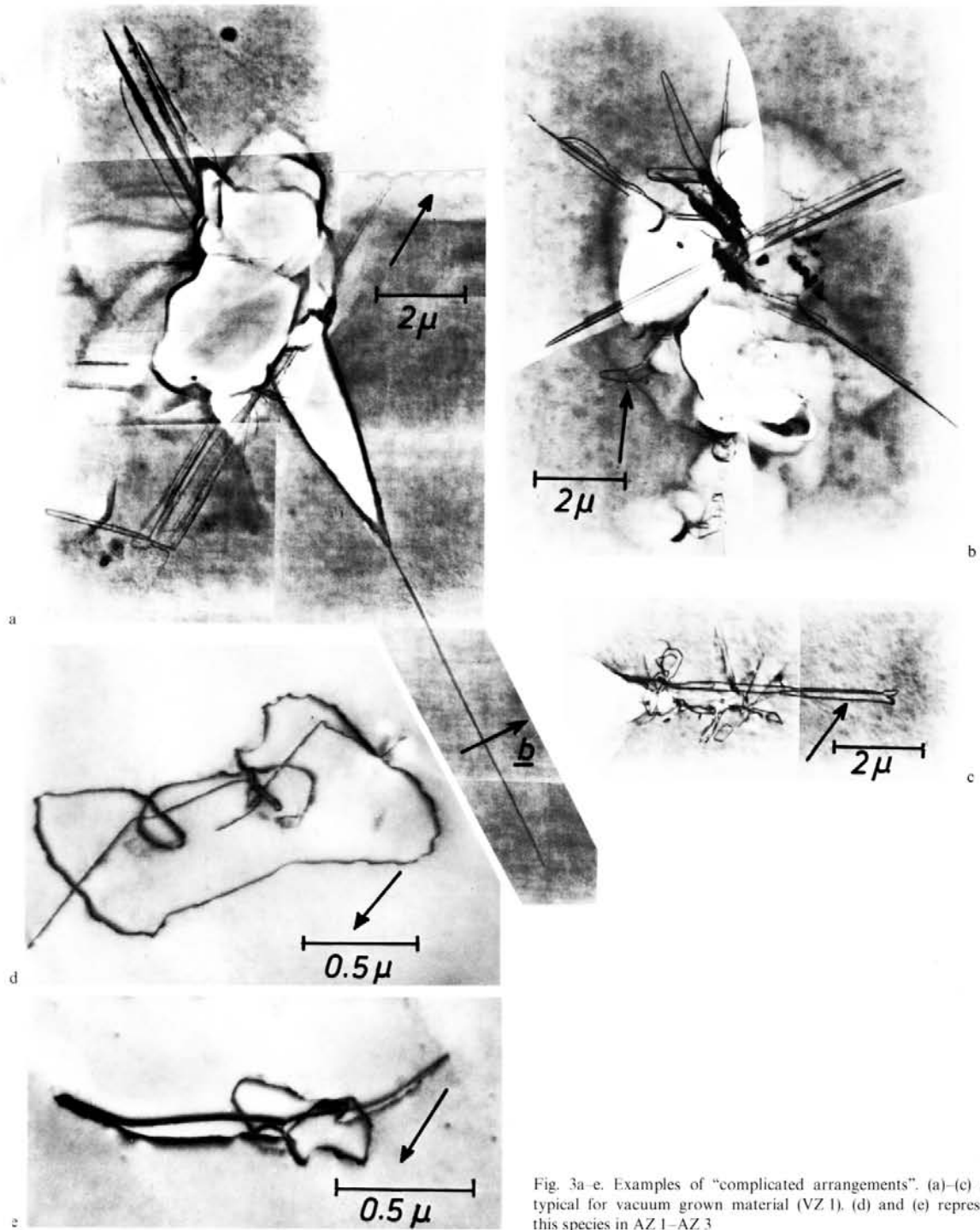


Fig. 3a-e. Examples of "complicated arrangements". (a)-(c) are typical for vacuum grown material (VZ 1). (d) and (e) represent this species in AZ 1-AZ 3

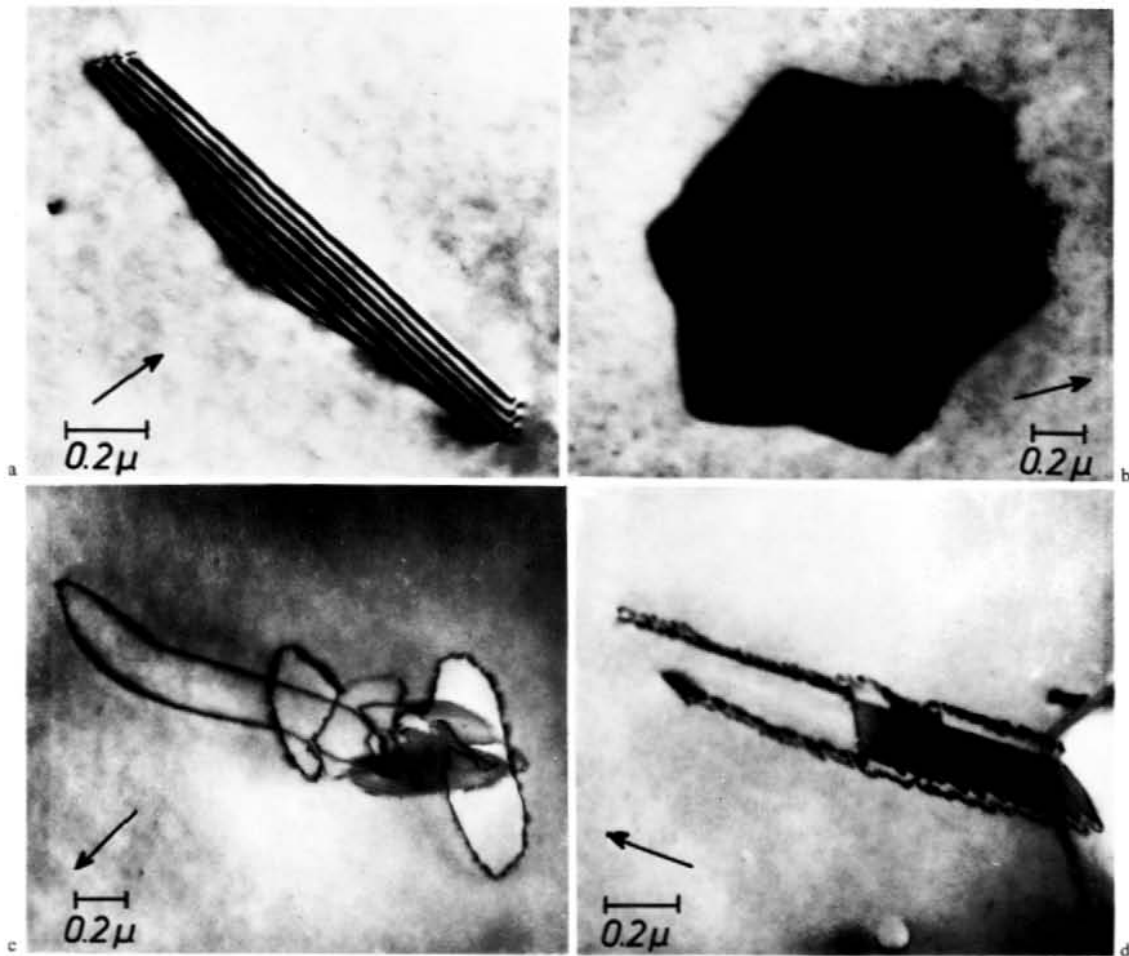


Fig. 4a-d. Typical examples of "faulted loops" observed almost exclusively in AZ 3 (a)-(c). (d) belongs to crystal AZ 2 (this was the only faulted loop which was not found in AZ 3)

2.3. Influence of Growth Rate on the Swirl Loops

In order to study the influence of growth rate a crystal (AZ 3) was pulled² increasing the growth rate v from $v=2$ mm/min to $v=5$ mm/min in steps of $\Delta v=0.5$ mm/min. The swirl distribution was revealed by etching techniques [6]. Using an optical microscope A- and B-swirls appeared as a striated pattern of etch-pits or hillocks. At higher magnifications the

² The authors are grateful to Dr. W. Keller of Siemens AG, Werk Halbleiter, Silizium-Entwicklung, München, for preparing this crystal.

etch-structures of the two types of swirls may be well distinguished (Fig. 6). A-swirls show relatively large etch-hillocks, whereas B-swirls appear as small shallow etch-pits. With increasing growth rate the distance between the rim and the first A-swirls increases from 1 mm (at $v=2$ mm/min) to 6 mm (at $v=3.5$ mm/min). At growth rates of 4 mm/min or larger, the A-swirls disappeared, whereas B-swirls are present up to growth rates of $v=4.5$ mm/min, in agreement with the observations of de Kock *et al.* [5]. The TEM investigations of the crystal AZ 3 yielded

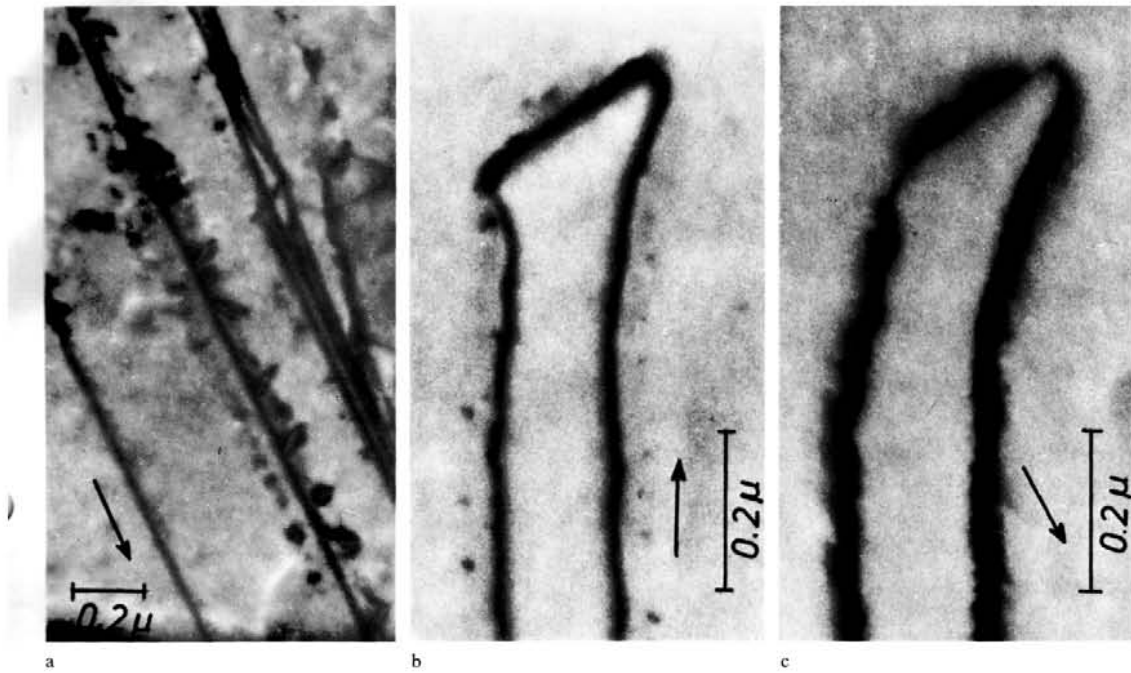


Fig. 5a-c. Examples of swirl-loop decoration. (a) shows small loops as found in VZ 1. (The related dislocations are *not* in contrast; the visible dislocation is *not* the decorated one). (b) and (c) show, respectively, "dots" and "hemlike contrast" of the same loop, depending on the diffraction conditions. Those contrasts are observed in AZ 1-AZ 3. The diffraction vector in (c) is of $\{111\}$ type

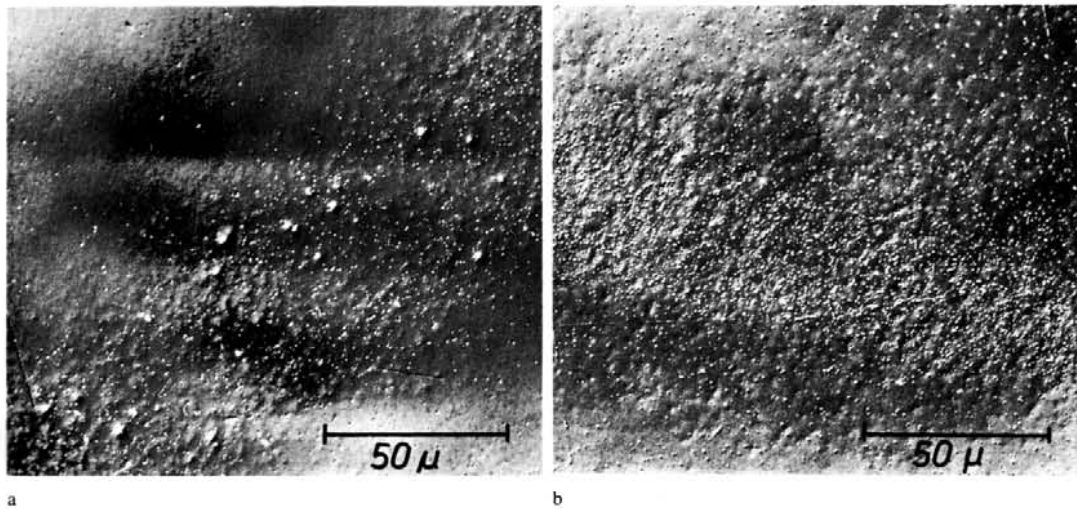


Fig. 6a and b. Etch patterns of swirls obtained by modified Sirtl etch treatment. (a) shows a swirl band containing A- and B-swirls. A-swirls show large hillocks; B-swirls appear as small shallow etch-pits. (b) shows a B-swirl band (distance from the rim ≈ 1 mm). No A-swirls are present in this region

the result that the size of the swirl loops is only weakly influenced by the growth rate. With increasing growth rate the mean size decreases from $\sim 1 \mu\text{m}$ ($v = 2 \text{ mm/min}$) to $0.5 \mu\text{m}$ ($v = 3.5 \text{ mm/min}$). Single loops are dominating, but loop clusters, complicated arrangements and especially faulted loops are also observed.

Even in specimens prepared from a dense B-swirl band no observable defects could be detected in the HVEM although the shallow etch-pits, indicating the B-swirl band, were easily found.

3. Analysis of the Loop Type

3.1. Outline of the Method

The analysis of the type (interstitial or vacancy) of a dislocation loop is commonly performed by application of the "inside-outside contrast" method [21, 22]. In the case of loops with a perfect Burgers vector (and therefore often not of pure edge-character) the rules derived for pure edge loops should not be applied indiscriminately [23, 24]. Föll and Wilkens [15] could recently show that the analysis of faulted and unfaulted loops is best performed using the sign convention for the Burgers vector introduced by Kröner [25] and Kroupa [26]. The analysis involves the following steps:

- i) Determine the axis of the normal \mathbf{n} of the loop plane³.
- ii) Determine the axis of the Burgers vector \mathbf{b} by conventional contrast experiments.
- iii) Determine the direction of \mathbf{b} by inside-outside contrast experiments using the $(\mathbf{g} \cdot \mathbf{b}) \cdot s$ -rules ($s =$ excitation error)

$$\text{inside contrast} \Rightarrow (\mathbf{g} \cdot \mathbf{b}) \cdot s > 0$$

$$\text{outside contrast} \Rightarrow (\mathbf{g} \cdot \mathbf{b}) \cdot s < 0.$$

- iv) Deduce sign $(\mathbf{n} \cdot \mathbf{b})$ from i) to iii) and obtain loop type from the relations

$$\mathbf{n} \cdot \mathbf{b} > 0 \Rightarrow \text{vacancy-type}$$

$$\mathbf{n} \cdot \mathbf{b} < 0 \Rightarrow \text{interstitial-type}.$$

3.2. Analysis of Single Loops and Loops in Loop Clusters

The method outlined in Section 3.1 was applied to single loops and loops in loop clusters. The loop normal \mathbf{n} may be determined by stereo micrographs

³ \mathbf{n} pointing upwards and loop viewed from above. In this paper all micrographs are printed emulsion side up.

and/or by large-angle tilting experiments – provided the loop or the main part of the loop is planar. An analysis was only carried out if the loop normal \mathbf{n} could be deduced unambiguously from stereo micrographs and large angle tilting experiments.

The Burgers vector of large loops may be determined by conventional contrast experiments, provided one takes into account that because of the decoration with small loops the contrast may not vanish completely at $\mathbf{g} \cdot \mathbf{b} = 0$ conditions (cf. Fig. 7a).

The inside-outside change of the contrast may be most clearly seen using a high-indexed reflexion ($\{422\}$ -type); inside-outside experiments were also performed with $\{220\}$ -reflexions and found to be consistent with the $\mathbf{g} = \{422\}$ results. A typical example of an analysed loop together with a schematic drawing of the contrast at different reflexions is shown in Fig. 7⁴. One recognizes that $\mathbf{n} \cdot \mathbf{b} < 0$; the loop is therefore of interstitial type. This result was obtained without exception for about 20 loops analysed.

3.3. Analysis of the Small Loops

The type of the small loops that could be resolved was determined. By performing large-angle tilting experiments it was found that the loop planes are near $\{111\}$. This is expected because loops in this size range are commonly located on or near $\{111\}$ planes – presumably because they originate from point-defect agglomeration on these planes.

With all diffraction vectors except that used in Fig. 8, the decorated dislocation is in contrast, and its image masks that of the small loops. Therefore contrast experiments could not be performed and it was not possible to determine unambiguously the Burgers vector of these loops. In the following we take into account that the loops may be faulted or unfaulted. That means, we have to consider all possible Burgers vectors. If we assume that the loops were created by point-defect agglomeration on a – as an example – $(11\bar{1})$ plane we have four possibilities for the Burgers vector

$$\mathbf{b}_{\text{imperf.}} = \pm a/3 [11\bar{1}]$$

$$\mathbf{b}_{\text{perf.}} = \pm a/2 \begin{cases} [10\bar{1}] \\ [110] \\ [01\bar{1}] \end{cases}$$

The $\langle 110 \rangle$ -type Burgers vectors may result from a shearing process, removing the stacking fault of the

⁴ All micrographs shown are taken with excitation error $s > 0$.

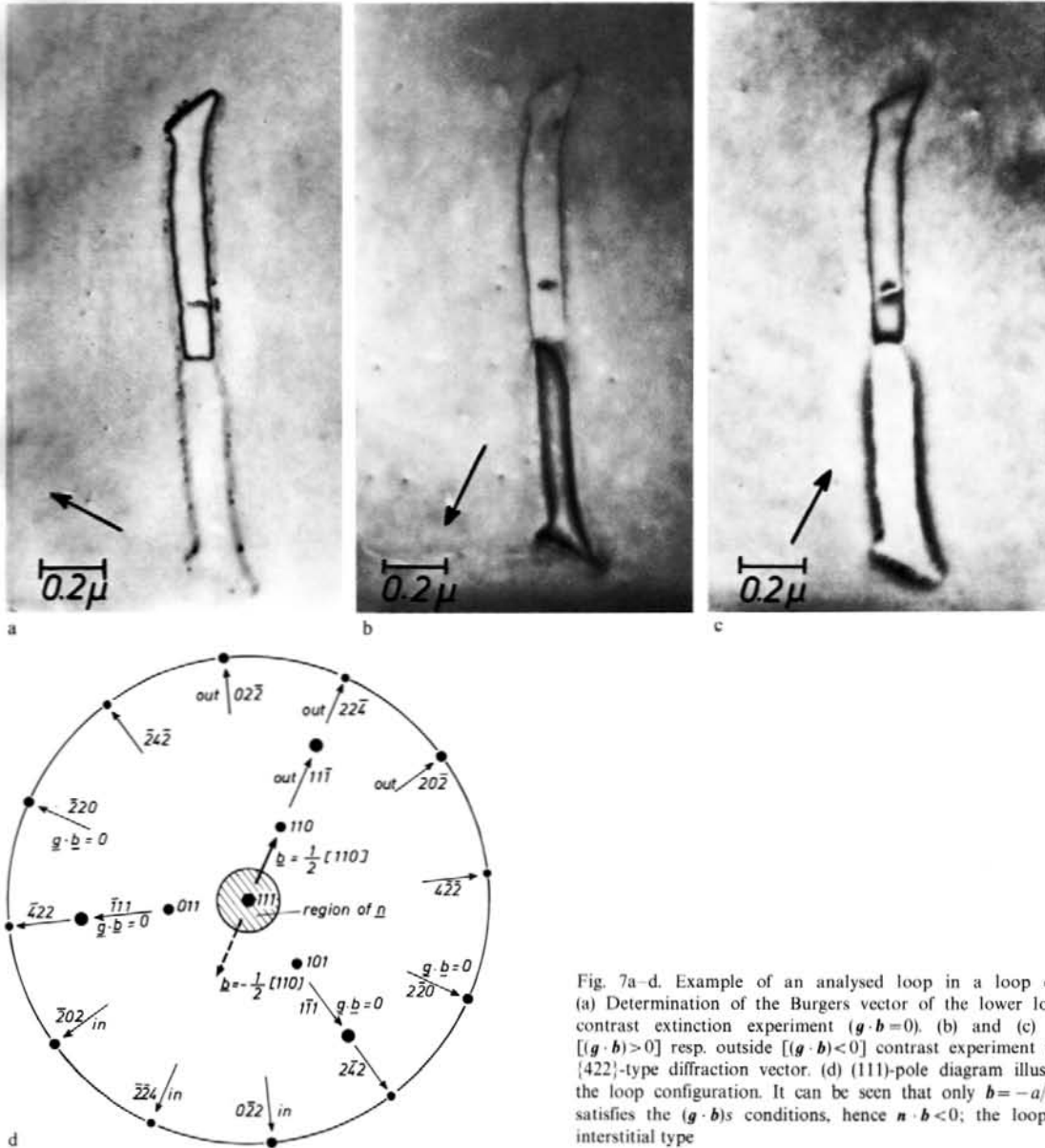


Fig. 7a-d. Example of an analysed loop in a loop cluster. (a) Determination of the Burgers vector of the lower loop by contrast extinction experiment ($g \cdot b = 0$). (b) and (c) Inside [$(g \cdot b) > 0$] resp. outside [$(g \cdot b) < 0$] contrast experiment with a $\{422\}$ -type diffraction vector. (d) (111)-pole diagram illustrating the loop configuration. It can be seen that only $b = -a/2[110]$ satisfies the $(g \cdot b)$ s conditions, hence $n \cdot b < 0$; the loop is of interstitial type

(originally) faulted loop. Figure 8, together with a schematical outline of the pole diagram, may illustrate this. It can be seen that we have $n \cdot b < 0$ for all four Burgers vectors; the loops are therefore of interstitial type. As already mentioned in [11], this contradicts earlier results [10], but one of the present authors (B.O.K.) found the earlier analysis to be incorrect.

3.4. Analysis of Faulted Loops

Loops including a stacking fault can be analysed applying the method described in Section 3.1. If a part of the loop is etched away (see Fig. 4a), the stacking fault ends at the surface and standard methods (see, e.g., [27]) may be applied. In all cases faulted loops were found to be of interstitial type.

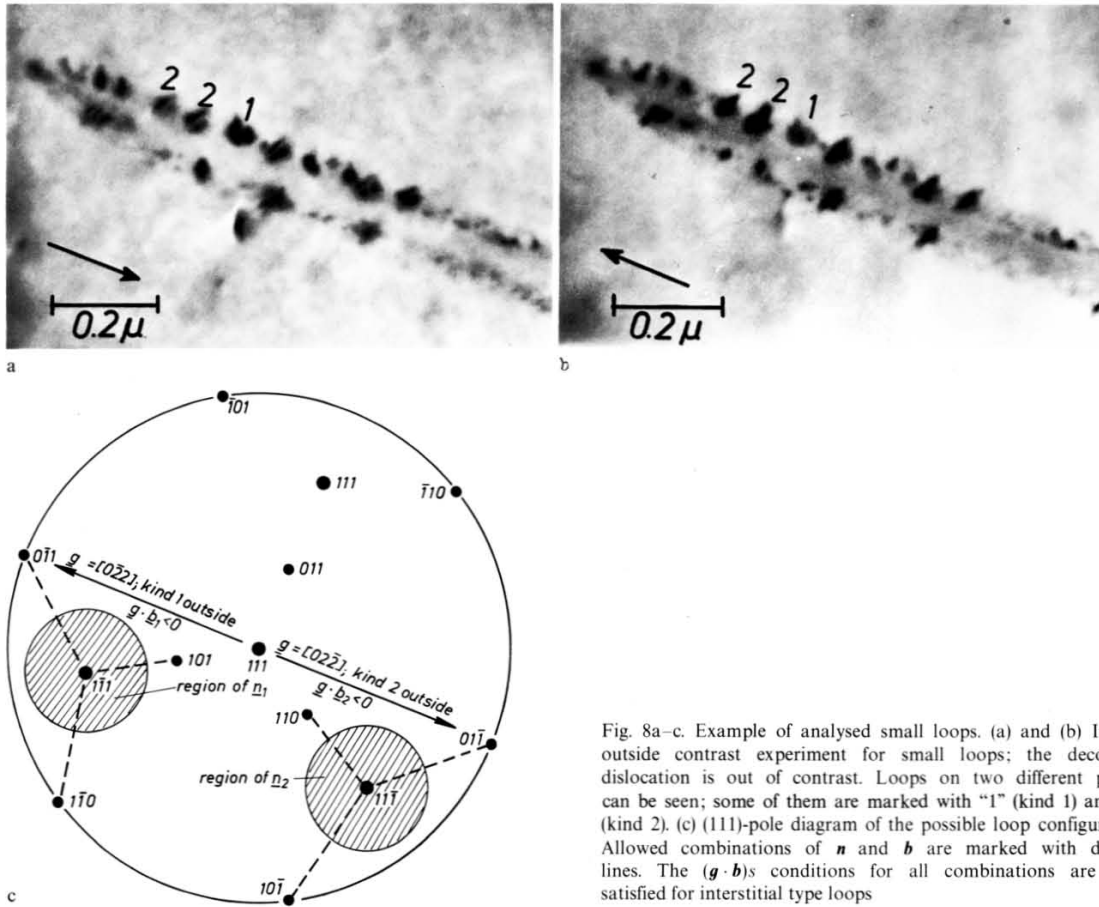


Fig. 8a-c. Example of analysed small loops. (a) and (b) Inside-outside contrast experiment for small loops; the decorated dislocation is out of contrast. Loops on two different planes can be seen; some of them are marked with "1" (kind 1) and "2" (kind 2). (c) (111)-pole diagram of the possible loop configuration. Allowed combinations of n and b are marked with dashed lines. The $(g \cdot b)$ s conditions for all combinations are only satisfied for interstitial type loops

4. Discussion

4.1. Comparison with Earlier Results

The interstitial nature of swirl loops found in this paper is in contrast to the assumptions made by other authors [28, 2] who considered swirls to be vacancy clusters. This assumption was made in analogy to f.c.c. metals. To our knowledge, valid experimental evidence for the vacancy nature of swirls was never published.

In swirl-rich regions α -cristobalite, i.e. a modification of SiO_2 , has been found by Ravi and Varker [8]. Since a small dislocation loop may act as a trap for oxygen, oxygen atoms as well as self-interstitials may be trapped by the loop. If the oxygen concentration is high enough, the amount of oxygen trapped at the loop may be comparable with the number of self-

interstitials, thus allowing SiO_2 precipitation. Data on the oxygen content were not given, but it seems likely that it was higher than in our specimens, because the oxygen precipitation indicates that its solubility (e.g. $4 \cdot 10^{17} \text{ cm}^{-3}$ at 1240°C [29]) was exceeded.

In another paper Ravi and Varker [30] reported that in swirl-rich regions of a crystal extrinsic stacking faults occur after an oxidation treatment, arranged in a striated pattern similar to swirls. The authors demonstrated that these faults do not arise from dislocation reactions but by agglomeration of self- or foreign interstitials. Assuming that vacancies are the point defects present at high temperatures, the authors had to make non-convincing assumptions in order to explain the origin of these interstitial type faults. In our opinion these faults may be created by accumula-

tion of oxygen and self-interstitials during the oxydation process. The stacking fault may be able to grow to a considerable size because it is stabilized by the precipitated oxygen (see below).

4.2. Some Remarks on the Occurrence of Faulted Loops

Faulted loops were only observed in the crystal with the highest impurity content (AZ 3). As will be outlined below, faulted loops of those large diameters should not be stable but should remove their stacking fault by a shearing process, according to, e.g.,

$$\mathbf{b}_F + \mathbf{b}_S = \mathbf{b}_{VF}$$

$$a/3[111] + a/6[11\bar{2}] = a/2[110],$$

where \mathbf{b}_F and \mathbf{b}_{VF} are the Burgers vectors of the faulted and unfaulted loops, respectively, and \mathbf{b}_S the Burgers vector of the Shockley partial. The reason for the unfaulting is that with increasing diameter d the energy of a faulted loop increases quadratically, but that of an unfaulted loop about linearly. The critical diameter d_c of which shearing should start is approximately proportional to $(|\mathbf{b}_{VF}|^2 - |\mathbf{b}_F|^2) \cdot G/\gamma$; where γ is the stacking fault energy and G the shear modulus. As it is known from metals with comparable G/γ -values, d_c is of the order of magnitude of a few hundred Å [31], hence the same can be expected for silicon.

It is well known that large stacking faults (several μm in length) may be formed in silicon when impurities such as oxygen [30, 32] or carbon [33] are involved in the formation process. Our results also suggest that these impurities are responsible for the stabilization of the faulted loops observed in crystal AZ 3. This implies that carbon and/or oxygen are incorporated into the stacking faults.

4.3. B-Swirls and the Nucleation of Swirls

The nucleation model proposed in the past [2] was conceived for vacancy condensation and has to be revised to apply to interstitial type clusters. A difficulty in establishing a general model for the formation of swirls lies in the fact that direct evidence on the nature of B-swirls is still missing. Recent investigations of de Kock *et al.* [5] appear to indicate that B-swirls are for-runners of A-swirls. In principle the fact that no B-swirls could be observed in the HVEM may have two reasons: Either that they are dislocation loops with diameters $\leq 200 \text{ \AA}$ ⁵ or that they consist of loose

⁵ This detection limit (which is well above the resolution limit of the microscope) may be estimated taking into account the low density of the B-swirls and the large thickness of the specimen.

agglomerates of self-interstitials and/or impurity atoms without a strong strain field, thus giving no detectable contrast in the HVEM. In the first case B-swirls simply should be identified with small A-swirls (swirl loops). If this were the case, it would be unclear why the majority of them do not become large. Furthermore there exists direct evidence that B-swirls are quite different in character from A-swirls. This may be concluded from the observations:

- i) B-swirls differ from A-swirls with regard to decoration with Cu or Li [2].
- ii) The spatial distribution of B-swirls is different from that of A-swirls (e.g., B-swirls occur nearer to the rim).
- iii) The influence of growth rate variations on the density and spatial distribution of B-swirls differ from those of A-swirls [2, 5].

Hence the remaining explanation is that B-swirls are agglomerates of self-interstitials and impurity atoms and can be considered as an embryonic stage of A-swirls.

The experimental observations provide strong indications that the nucleation of A-swirls, and therefore also of B-swirls, is heterogeneous:

- i) The density of A-swirls increases with increasing impurity content. Crystal VZ 1 with an impurity content (oxygen and carbon) one or two orders of magnitude below that of crystal AZ 1 shows a swirl density which is about a factor of 10 smaller than of crystal AZ 1.
- ii) The swirl pattern exhibits pronounced striations of the swirl density which is correlated to the striated incorporation of impurities with segregation coefficients $k < 1$ (e.g., P, C).

The nucleation site may be an association of self-interstitials and oxygen and/or carbon since oxygen and carbon are effective traps for self-interstitials [34] and constitute the dominating impurities in silicon apart from intentionally incorporated elements [35]. Especially the participation of carbon might give a reasonable explanation for the striated distribution of swirls, since because of its distribution coefficient $k \approx 0.05$ [36] carbon is always distributed inhomogeneously [37]. By contrast, according to recent investigations of Vieweg-Gutberlet [7] oxygen is incorporated more uniformly.

The reduction of the mean diffusion distance of the self-interstitials resulting from an increase of the growth rate from 3.5 to 4 mm/min is only about 15% and can therefore not account for the total disappearance of A-swirls in this growth rate range. The

disappearance might rather be due to an impeding of the collapse of the B-swirls at higher growth rates. Provided that B-swirls are three-dimensional clusters of interstitial atoms they act as centers of compression which, compared to dislocation loops, interact weakly with interstitials. Since, due to the decrease of temperature, the time available for the growth of B-swirls is restricted, they remain small. An increase of the growth rate (which corresponds to a faster rate of temperature decrease) may suffice to reduce their size below the limit required for a conversion to a dislocation loop. If thermal activation favours this conversion, higher growth rates will suppress it even more.

4.4. A model for Formation of Swirl-Loops

This model starts with the formation of small, faulted dislocation loops on $\{111\}$ -planes. This can be achieved by a conversion of B-swirls (see above). The formation of the observed swirl loops consists of the following steps:

a) By association of self-interstitials the small faulted loops grow up to the critical diameter d_c , where the shearing process occurs. Depending on the impurity content of the crystal, a certain amount of impurities is also trapped by the loop. As outlined in Section 4.2, the impurity concentration in the fault determines d_c . At fairly high impurity contents (at least 10^{17} cm^{-3} , cf. Section 4.1) the number of impurity atoms joining the dislocation loops at a given time may be comparable with the number of self-interstitials. As a result a precipitate is formed.

b) The elimination of the stacking fault by the shearing process leads to an undisturbed lattice within the loop. The impurities which were trapped in the fault become mobile again. Thus each shearing process results in an "ejection" of an "impurity cloud" which surrounds the (perfect) dislocation loop. Hence the probability of forming new nuclei in the neighbourhood of the loop is strongly increased. New loops are formed, grow and undergo shearing processes which lead to new nuclei again. The resulting loop multiplication process may occur several times depending on the critical size at which the shearing process starts. As a consequence stacking faults should exist only as single loops or in connection with several perfect loops and not as a cluster of faulted loops. This is in accordance with our observations (see Fig. 4). If the impurity content is low, the shearing process occurs at small diameters of the loop. Thus in very pure crystals (VZ 1) loop multiplication can take place

more frequently than in crystals with higher impurity content. According to our results, we expect therefore an increase of the complexity of the swirl loops with decreasing impurity content. On the other hand, at fairly high impurity contents the faulted loops can grow to a considerable size and the shearing process may even sometimes be suppressed. Single loops and faulted loops will be the dominating species in such crystals. It should be kept in mind that with decreasing temperature of the crystal the concentration and mobility of the point defects decreases and the different processes (nucleation, shearing, etc.) are stopped. Therefore different stages of swirl loops are "quenched in", including faulted loops as in crystal AZ 3.

c) During the growth of the loops different mechanisms may influence their shape. Due to temperature and stress gradients and due to the lower energy of a dislocation along $\langle 110 \rangle$, the loops get an elongated shape with the main parts of the dislocation parallel to $\langle 110 \rangle$. With increasing size of the loop it becomes energetically more favourable to lower the angle between \mathbf{n} and \mathbf{b} (which is $\approx 35^\circ$ after shearing). The corresponding reorientation process [24, 38] can only start at the tips of the loop, therefore the tips are often near a pure edge configuration (cf. Section 2.2). Furthermore, plastic processes due to internal stresses may occur, changing the shape of the swirl loops by conservative glide and especially by climb of the dislocations.

d) Due to the repeated shearing processes which set free the impurities bound in the stacking fault and due to additional trapping of impurities along the dislocation line the probability for the formation of new nuclei rises during the final stage of swirl loop formation. The loops formed at these nuclei remain small because mobility and concentration of self-interstitials have decreased (the decrease in concentration is due to the incorporation of the self-interstitials into the swirl loops) and moreover the number of nuclei is high because of the increased impurity concentration. Thus even precipitation might take place. The stress field of the large dislocation loop favours the growth of those loops located on the outer side of the large loops (i.e. in the dilatation area). This may be an explanation for the observation that the small loops are almost exclusively found on the outer side of the large loops (cf., e.g., Fig. 5b). In accordance with our observation faulted loops should exhibit a lower degree of decoration with small loops, because the main part of the impurities is still trapped in the stacking fault.

e) Apart from oxygen and carbon, other impurities, in particular fast diffusing metals like Cu or Au may be trapped by the swirl loops. For example, Au-contents of about 10^{13} cm^{-3} are sufficient to result in a preferential precipitation of Au at the swirls, which can be revealed by autoradiography techniques [39]. In accord with the low content of heavy metals no decoration of the loops with precipitates could be detected in our crystals.

Acknowledgements. The authors are grateful to Drs. J. Burtcher, W. Frank, K. Mayer, A. Seeger, H. Strunk, K. Urban, and M. Wilkens for many helpful discussions and for critical reading of the manuscript. They also would like to thank Mrs. H. Mylonas and G. Schuh for specimen preparation and Miss L. Holl for the careful photographic work. The support by the Stiftung Volkswagenwerk, which financed the high-voltage electron microscope, is gratefully acknowledged.

References

1. E. Sirtl, A. Adler: *Z. Metallkunde* **52**, 529 (1961)
2. A. J. R. de Kock: *Philips Res. Repts. Suppl.* **1**, (1973)
3. C. J. Varker, K. V. Ravi: *J. Appl. Phys.* **45**, 272 (1974)
4. J. Chikawa, Y. Asaeda, I. Fujimoto: *J. Appl. Phys.* **41**, 1922 (1970)
5. A. J. R. de Kock, P. J. Roksnoer, P. G. T. Boonen: *J. Crystal Growth* **22**, 311 (1974)
6. L. I. Bernowitz, K. R. Mayer: *Phys. Stat. Sol. (a)* **16**, 579 (1973)
7. F. Vieweg-Gutberlet: *Spreading Resist. Symp. Nat. Bur. Stands. Special Publ.*, Gaithersburg (1974), p. 185
8. K. V. Ravi, C. J. Varker: In *Semiconductor Silicon* 1973, ed. by H. R. Huff and R. R. Burgess (The Electrochem. Soc. Softbound Symposium Series, Chicago 1973), p. 83
9. L. I. Bernowitz, B. O. Kolbesen, K. R. Mayer, G. E. Schuh: *Appl. Phys. Lett.* **25**, 277 (1974)
10. H. Griener, B. O. Kolbesen, K. R. Mayer: In *Lattice Defects in Semiconductors*, Freiburg 1974, Inst. of Phys. Conf. Series No. **23**, 531 (1975)
11. H. Föll, B. O. Kolbesen, W. Frank: *Phys. Stat. Sol. (a)* **29**, K 83 (1975)
12. A. Seeger, M. L. Swanson: In *Lattice Defects in Semiconductors*, ed. by R. R. Hasiguti (University of Tokyo Press, Tokyo, and Pennsylvania State University, University Park and London 1968), p. 93
13. A. Seeger, K. P. Chik: *Phys. Stat. Sol.* **29**, 455 (1968)
14. A. Seeger: *Radiat. Effects* **9**, 15 (1971)
15. H. Föll, M. Wilkens: To be published in *Phys. Stat. Sol.*
16. H. Neubrand: *Phys. Stat. Sol. (a)* **17**, 459 (1973)
17. B. O. Kolbesen, K. R. Mayer, G. E. Schuh: *J. Phys. E (Scientific Instrum.)* **8**, 197 (1975)
18. G. R. Booker, R. Stickler: *Brit. J. Appl. Phys.* **13**, 446 (1962)
19. R. S. Nelson: In *Radiation Damage and Defects in Semiconductors*, Reading 1972, Inst. of Phys. Conf. Series No. **16**, 140 (1973)
20. H. Föll: In *Lattice Defects in Semiconductors*, Freiburg 1974, Inst. of Phys. Conf. Series No. **23**, 233 (1975)
21. G. W. Groves, A. Kelly: *Phil. Mag.* **6**, 1527 (1961)
22. D. J. Mazey, R. S. Barnes, A. Howie: *Phil. Mag.* **7**, 1861 (1962)
23. D. M. Maher, B. L. Eyre: *Phil. Mag.* **23**, 409 (1971)
24. P. M. Kelly, R. G. Blake: *Phil. Mag.* **28**, 415 (1973)
25. E. Kröner: *Kontinuumstheorie der Versetzungen und Eigenspannungen* (Springer-Verlag, Berlin, Göttingen, Heidelberg 1958)
26. F. Kroupa: *Czech. J. Phys.* **A13**, 301 (1963)
27. P. B. Hirsch, A. Howie, R. B. Nicholson, D. W. Pashley, M. J. Whelan: *Electron Microscopy of Thin Crystals* (Butterworth, London 1965), p. 235
28. T. S. Plaskett: *Trans. AIME* **233**, 809 (1965)
29. Y. Takano, M. Maki: In *Semiconductor Silicon* 1973, ed. by H. R. Huff and R. R. Burgess (The Electrochem. Soc. Softbound Symposium Series, Chicago 1973), p. 469
30. K. V. Ravi, C. J. Varker: *J. Appl. Phys.* **45**, 263 (1974)
31. J. A. Sigler, D. Kuhlmann-Wilsdorf: *Phys. Stat. Sol.* **21**, 545 (1967)
32. S. M. Hu: *J. Appl. Phys.* **45**, 1567 (1974)
33. R. Ogden, R. R. Bradley, B. E. Watts: *Phys. Stat. Sol. (a)* **26**, 135 (1974)
34. G. D. Watkins: In *Lattice Defects in Semiconductors*, Freiburg 1974, Inst. of Phys. Conf. Series No. **23**, 1 (1975)
35. J. Burtcher: In *Scientific Principles of Semiconductor Technology*, ed. by H. Weiß, Proc. of the Europ. Summer School, Bad Boll, Germany (1974) p. 63
36. T. Nozaki, Y. Yatsurugi, N. Akiyama: *J. Electrochem. Soc.* **117**, 1566 (1970)
37. T. Abe, Y. Abe, J. Chikawa: In *Semiconductor Silicon* 1973, ed. by H. R. Huff and R. R. Burgess (The Electrochem. Soc. Softbound Symposium Series, Chicago 1973), p. 83
38. O. G. Bacon, A. G. Crocker: In *Lattice Defects in Quenched Metals*, ed. by R. M. Cotterill, M. Doyama, J. J. Jackson, and M. Meshii (Academic Press, New York 1965) p. 667
39. E. Haas, K. R. Mayer, M. Schnöller: In *Forschungsbericht NT 74 DK 5462805: 6213822/3* (1973) Bundesministerium für Forschung und Technik, Fed. Rep. Germany